Journal of Rheology

RESEARCH ARTICLE | NOVEMBER 20 2025

Slit-rheometry-based characterization of the flow behavior of diluted polymer melts

Ernst Georg Viehböck ; Alexander Hammer ; Markus Kirchmayr ; Christof Murnig ; Christian Paulik ; Gerald Berger-Weber

J. Rheol. 70, 35–45 (2026)
https://doi.org/10.1122/8.0001059

Slit-rheometry-based characterization of the flow behavior of diluted polymer melts

Ernst Georg Viehböck,[1,2,a)] Alexander Hammer,[2] Markus Kirchmayr,[3] Christof Murnig,[4] Christian Paulik,[1,5] and Gerald Berger-Weber[2]

[1]*Competence Center CHASE GmbH, Hafenstraße 47-51, 4040 Linz, Austria*
[2]*Institute of Polymer Processing and Digital Transformation, Johannes Kepler University Linz, Altenberger Straße 69, 4040 Linz, Austria*
[3]*EREMA Engineering Recycling Maschinen und Anlagen Ges.m.b.H., Unterfeldstraße 3, 4052 Ansfelden, Austria*
[4]*GAW Technologies GmbH, Puchstraße 76, 8020 Graz, Austria*
[5]*Institute of Chemical Technology of Organic Materials, Johannes Kepler University Linz, Altenberger Straße 69, 4040 Linz, Austria*

(Received 13 June 2025; final revision received 15 September 2025; published 20 November 2025)

Abstract

Polymer melts that are diluted, that is, to which low-molecular-weight diluents have deliberately been added to modify them, have attracted growing interest due to their ability to significantly reduce melt viscosity, thereby improving processability and enhancing extrusion efficiency. We present a novel experimental setup based on slit rheometry that integrates a slit rheometer with a single-screw extruder, a gear pump, and a high-pressure liquid chromatography pump for diluent injection. A distinctive feature of this setup is its adjustable diluent injection point, which allows systematic investigation of the impact of injection location on in-line mixing, diluent incorporation, and the resulting rheological behavior under high-pressure processing conditions. In order to mitigate diluent evaporation or bubble nucleation, the Antoine equation is used to determine the pressure under which the setup operates. Experimental results demonstrated that adding n-decane to high-density polyethylene substantially reduced viscosity, with direct injection into the extruder yielding lower measurement variability and a higher saturation threshold than injection downstream of the melt pump. This advanced method offers a robust framework for determining rheological properties of diluted melts to enhance process design and optimization. https://doi.org/10.1122/8.0001059

I. INTRODUCTION

Diluted polymer melts—polymer systems modified by the addition of diluents—have attracted significant attention in polymer processing because of their potential to reduce melt viscosity and thus improve processability, equipment design, and extrusion efficiency. Early studies laid the groundwork for this field by exploring viscosity reduction in various polymer–diluent systems. For instance, Spencer and Williams [1] reported first measurements of viscous polystyrene solutions in toluene, demonstrating a strong dependence of viscosity on polymer concentration. Fujita and Maekawa [2] advanced the theoretical understanding of viscosity reduction with his free-volume theory for diffusion in polymer–diluent systems, while Graessley [3] introduced the entanglement concept to explain the abrupt viscosity increase observed in concentrated solutions. Nishimura [4] derived a general relationship between viscosity and polymer concentration, and Brockmeier and Westphal [5] investigated high-density polyethylene (HD-PE) solutions in aliphatic solvents such as decalin, establishing models for predicting viscosity behavior of the mixture. Subsequent work by Ide and White [6] focused on polystyrene systems in the presence of styrene, and Mendelson [7] developed high-pressure capillary rheometry techniques to study polystyrene in styrene and other volatile solvents. Foster and Lindt [8] contributed by designing a high-pressure viscometer for polystyrene/ethylbenzol solutions, highlighting the influence of both temperature and pressure on the rheological properties of diluted systems. Numerous studies on foaming with supercritical fluids have investigated the influence of these gases on polymer rheology, providing insights that also apply to studies on liquid diluents. For instance, Fernández-Ronco *et al.* [9], Han and Ma [10], Royer *et al.* [11], Kwag [12], Gerhardt *et al.* [13,14], and Lee *et al.* [15] focused primarily on supercritical CO_2, demonstrating its capacity to markedly reduce polymer viscosity under high-pressure conditions. Studies by Ma and Dae Han [16], Areerat *et al.* [17], Handge and Altstädt [18], and Qin *et al.* [19] examined the rheological behavior of polymers in the presence of supercritical N_2. These seminal works not only elucidated the mechanisms of diluent-induced viscosity reduction, but also underscored the importance of operating in a controlled high-pressure environments—a concept that underlies the present study on liquid low-molecular-weight diluents.

Accurate rheological measurements are critical not only for establishing baseline material properties, but also for

a)Author to whom correspondence should be addressed: electronic mail: ernst.viehboeck@chasecenter.at

modeling and simulation of polymer processes. Using conventional rheometry techniques—such as parallel-plate and high-pressure capillary rheometry—is state of the art when the rheological behavior of the neat polymer melt is to be characterized. However, due to (i) undesired evaporation of low-molecular-weight diluents, (ii) the need to operate under high-pressure conditions, and (iii) difficulties in achieving reproducible mixing in offline saturation often render these approaches inadequate when applied to diluted polymer systems.

Various experimental approaches have been developed to characterize the rheological behavior of diluted polymer melts. Modified capillary rheometers [7,20] and dual-piston (multipass) capillary rheometers [21–23] enable measurement at high shear rates, and parallel-plate rheometers [18,24] provide controlled oscillatory shear testing, but all these methods are frequently hampered either by diluent evaporation at elevated processing temperatures or by inconvenient pressure seals. Alternative techniques, such as magnetically levitated sphere rheometers [25], have been introduced, but they have issues regarding mixing and are typically limited to less viscous systems. More recently, extrusion rheometers [26,27] have emerged as a promising solution, as they enable rheological characterization under conditions that closely mimic industrial processing, including high-pressure environments and continuous flow.

Although polymer–diluent systems have been studied in various contexts, little systematic investigation has been done of the rheological properties of PE-HD containing *n*-decane—under processing conditions where evaporation is a critical concern. To prevent diluent volatilization, the system must operate at a pressure level specific to the polymer–diluent combination, which can be determined using the Antoine equation [28]. This semiempirical relationship describes the dependence of vapor pressure on absolute temperature for a given substance. Presaturating the polymer granules with diluent before processing is inherently unfeasible, as exposure to elevated temperatures during melting inevitably leads to evaporation of some of the diluent, altering its concentration. Consequently, in-line mixing capabilities are essential to ensuring consistent and reproducible dilution levels throughout an experiment. These stringent requirements—maintaining sufficient pressure, enabling viscosity measurements across a wide range of shear rates, and ensuring effective mixing—called for the development of a novel experimental setup. The setup we propose here integrates a lab-scale single-screw extruder with a high-performance liquid chromatography (HPLC) pump and a slit rheometer.

II. EXPERIMENTAL

A. Materials

The polymeric material used in this study was the PE-HD grade BB2581 (Borealis, Vienna, Austria), which was specifically designed for blow-molding applications. The material is characterized by a multimodal molecular-weight distribution and a melt-flow rate (MFR) of 0.3 g/10 min (190 °C/2.16 kg). To ensure chemical compatibility with polyethylene (PE), which is composed of ethylene monomer units, a linear alkane was selected as the diluent.

Inspired by Kastner [29], who investigated the diluting effects of eicosane (C20), we chose *n*-decane (purity $> 99\%$ by Sigma Aldrich, abbreviated as C10) as a low-molecular-weight ($142.28\,\mathrm{g\ mol^{-1}}$) diluent. Given its boiling point of 174.1 °C [30], *n*-decane would be expected to rapidly evaporate under typical PE-HD processing temperatures of 200 °C.

Since our objective was to describe vapor pressure behavior near and beyond ambient pressure evaporation, a simple Antoine fit was insufficient for the full temperature range. Instead, a numerical fitting procedure was performed on FLUIDAT® (Bronkhorst, The Netherlands) data spanning $0 - 300\,^{\circ}\mathrm{C}$ to determine accurate Antoine parameters for *n*-decane. This approach allows precise calculation of the minimum pressure required to prevent bubble nucleation at various processing temperatures. The Antoine equation is a semiempirical correlation that describes the relationship between vapor pressure P and absolute temperature T based on three substance-specific parameters A, B, and C,

$$\log_{10} P = A - \left(\frac{B}{T + C}\right). \tag{1}$$

In the supplementary material, the minimum pressure for the two processing temperatures is calculated.

Since later calculations required the melt density of the neat polymer, MFR (melt-flow rate) experiments were carried out with 2.16 kg load at 200 and 240 °C. The melt density was determined to be $0.746\,\mathrm{kg/m^3}$ at 200 °C and $0.728\,\mathrm{kg/m^3}$ at 240 °C.

B. Single-screw extruder

The PE-HD material was extruded using a lab-scale single-screw extruder (SSE) (Thermo Fisher Scientific, Waltham, MA, USA) with a diameter of 19 mm and an axial length of 33D. The extruder was equipped with a conventional three-zone screw and a smooth barrel featuring dedicated ports for pressure transducers or melt-temperature sensors located at 13D, 16D, 19D, 21D, 25D, and 33D. The extruder temperature was controlled by means of a water-cooled intake zone and electrically heated barrel and adapter zones.

C. Melt pump

A gear pump (Mahr, Göttingen, Germany) with a conveying capacity of $2.642\,\mathrm{cm^3}$ per revolution was utilized in selected experiments to regulate the volumetric flow rate of the extrusion rheometer.

D. Extrusion rheometer

The extrusion rheometer used in this study was based on a slit die with the following dimensions in the measuring section: width $W = 20$ mm, height $H = 1.2$ mm, and length $L = 75$ mm. The total length of the constant cross-sectional slit was 120 mm. The measuring section was instrumented with three pressure transducers located at 0, 50, and 75 mm,

and a noninvasive melt-temperature sensor at 25 mm to precisely monitor the pressure drops and melt temperatures at varying volume-flow rates. The first pressure transducer was positioned at least 20 mm downstream from the slit inlet to avoid entrance effects, and the last pressure transducer at $L = 75$ mm was still 25 mm (center-to-edge) from the downstream end of the slit.

E. Diluent pump

To inject the low-molecular-weight diluent (*n*-decane) into the polymer melt, a HPLC double-piston pump (BlueShadow 40P, Knauer, Berlin, Germany) was used. This pump is equipped with a stainless steel 10 ml/min pump head and is capable of operating at pressures of up to 65 MPa at a volume flow rate of 4 ml/min and up to 40 MPa at 10 ml/min. Additionally, a nonreturn valve protects the pump and capillaries from melt backflow from the extruder.

III. DESIGN OF EXPERIMENTSAL SETUP AND DATA PROCESSING

A. Experimental setup

The experimental setup combines the aforementioned component: the single-screw extruder, the gear pump (melt pump), the HPLC pump for diluent injection, and the slit rheometer in two different configurations, which allows adjusting the diluent injection point. As illustrated in Figs. 1 and 2, there are two distinct injection modes.

Injection Mode 1—Downstream of the Melt Pump (ER):

In this configuration (see Fig. 1, abbreviated as configuration ER), the diluent is injected downstream of the melt pump into a pure pressure flow region. Due to inherently limited mixing in this region, two static mixers (approximately 10 mm in diameter) (SMX™ by Sulzer, Winterthur, Switzerland) positioned downstream of the injection point to improve both material and thermal homogeneity.

Injection Mode 2—Directly into the Extruder (ER-IS):

Alternatively, the injection point can be shifted upstream such that the diluent is introduced directly into the extruder (ER-IS, see Fig. 2). This configuration provides flexibility to adjust the injection position to various locations along the screw.

This adjustable injection strategy is a key innovation of this setup because it allows systematic evaluation of how the injection position influences diluent incorporation, mixing, and ultimately the rheological behavior of diluted polymer melts. This is essential to achieving a homogeneous diluent distribution and reproducible measurements under relevant processing conditions.

B. Data evaluation

1. Slit rheometry

The well-known Hagen–Poiseuille equation analog for slit-flow was applied to determine viscosities from slit rheometry measurements. For a slit with constant cross-sectional shape, the wall shear stress τ_W was calculated based on the momentum balance with pressure drop Δp, slit width W, slit height H, and the length L of the measurement domain using the following equation, where the term in brackets accounts for the effect of lateral walls:

$$\tau_W = \frac{H\Delta p}{2L}\left(1+\frac{H}{W}\right)^{-1}. \tag{2}$$

The condition of fully developed flow was validated to ensure that the measurement results were not influenced by viscous dissipation, pressure-dependent viscosity, or diluent bubble nucleation. A linear pressure profile along the slit die is considered a reliable indicator of fully developed flow [31].

In addition, the absence of wall slip must be confirmed, since short-chain *n*-alkanes such as *n*-decane may act as lubricants at the polymer–wall interface. Wall-slip verification can be performed either by extrusion rheometry using slit dies of different heights or by parallel-plate measurements at varying gap widths. In the latter approach, as described by Yoshimura and Prud'homme [32], the occurrence of slip would manifest as a disproportionate reduction in torque with decreasing gap height. If slip is detected, the apparent shear rate $\dot{\gamma}_{\text{app}}$ must be corrected accordingly.

The apparent shear rate $\dot{\gamma}_{app}$ in a rectangular slit derived from the velocity profile for a Newtonian fluid is defined as

$$\dot{\gamma}_{app} = \frac{6Q}{WH^2}, \tag{3}$$

where Q is the overall volumetric flow rate. The Schümmer approximation by Schümmer and Worthoff [33] was used as

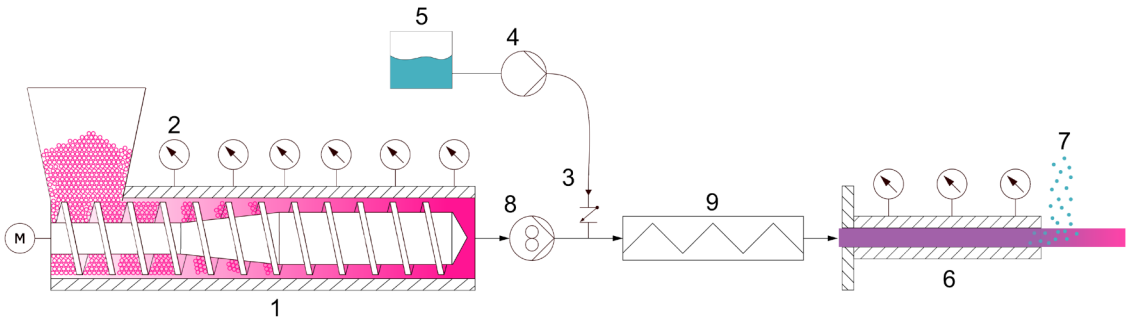

FIG. 1. Schematic overview of the extrusion rheometry setup with injection after the melt pump (ER). (1) Single-screw extruder, (2) pressure transducer, (3) check valve, (4) diluent pump, (5) diluent reservoir, (6) extrusion rheometer, (7) evaporation of the diluent, (8) melt pump, and (9) static mixers.

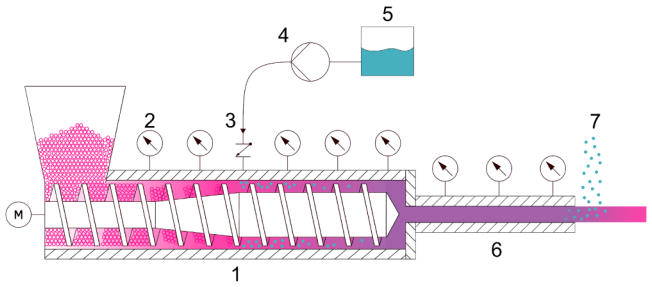

FIG. 2. Schematic overview of the extrusion rheometry with injection into the extruder (ER-IS). (1) Single-screw extruder, (2) pressure transducer, (3) check valve, (4) diluent pump, (5) diluent reservoir, (6) extrusion rheometer, and (7) evaporation of the diluent.

an approximation for the non-Newtonian shear rate at the wall the so-called approximate wall shear rate $\dot{\gamma}$. This approximation introduces a simple factor e, which depends on the cross-sectional shape of the die (rectangular, circle, ...) and the power-law index n,

$$\dot{\gamma} = \dot{\gamma}_{app} \cdot e, \tag{4}$$

$$e = \frac{3n}{2n+1}. \tag{5}$$

The resulting viscosity η at the Schümmer shear rate $\dot{\gamma}$ can then be written as

$$\eta = \frac{\tau_W}{\dot{\gamma}} = \frac{WH^3}{eQ12}\frac{\Delta p}{L}\left(1+\frac{H}{W}\right)^{-1}. \tag{6}$$

To better illustrate the dependence of viscosity on diluent concentration, a normalized viscosity $\tilde{\eta}$ is introduced, defined as

$$\tilde{\eta} = \frac{\eta_{dil}}{\eta_{undil}}, \tag{7}$$

where η_{dil} represents the diluted viscosity at a given diluent concentration and η_{undil} denotes theviscosity of the undiluted polymer melt at a given temperature and shear rate. Since the addition of diluents affects the throughput and thus the effective shear rate, a simple power-law model was applied to calculate η_{undil} at the exact same shear rate corresponding to the measurement of η_{dil}, thereby excluding the influence of shear-thinning effects.

The applied power-law model is given by

$$\eta(\dot{\gamma}) = K\dot{\gamma}^{n-1}, \tag{8}$$

where K is the consistency index, corresponding to the viscosity at a shear rate of $\dot{\gamma} = 1\,\mathrm{s}^{-1}$, and n is the power-law exponent.

Figure 3 presents a typical melt temperature profile in the slit rheometer for one arbitrarily chosen experiment. The melt temperature exhibits a sinusoidal variation with a maximum amplitude of less than 10 °C, which we attribute to nonoptimal control of the temperature of the die. The

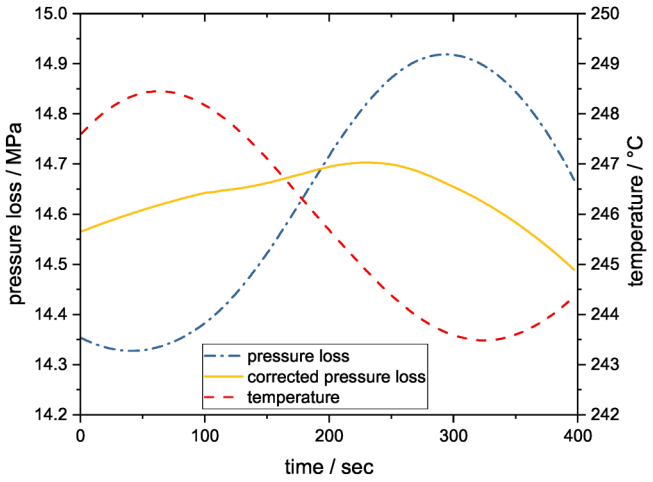

FIG. 3. Pressure and temperature fluctuations over time in ER. For improved readability, the data were smoothed using a Savitzky–Golay filter with a window size of 100 points and polynomial order of two. The original, unsmoothed data were used for all calculations; only the filtered data are shown here for clarity.

pressure loss in the die follows sinusoidally with a phase shift of 180 °. To ensure that the analysis remained independent of these temperature fluctuations, a temperature correction was applied: The approximate Arrhenius relation is a widely used method that uses exponential correction to compensate for small temperature variations,

$$\eta_{corr}(T_{ref}) = \eta_{meas}\exp(\beta(T_{ref} - T)), \tag{9}$$

where β is the temperature sensitivity coefficient of the viscosity, T_{ref} is the reference temperature, and T is the actual temperature of the melt. To determine the temperature sensitivity coefficient, a numerical fitting procedure was implemented. This approach aimed to minimize the standard deviation of the corrected pressure data across all measurements conducted in the absence of diluents. By iteratively adjusting β, the method ensured effective compensation for temperature-induced variations in pressure readings, thereby improving comparability of the experimental results.

C. Predicting the volume flow

Equation (6) requires the volumetric flow rate Q to be known. In the ER setup, this can be determined directly, as the melt pump consistently conveys a fixed volume of $V_{MP} = 2.642\,\mathrm{cm}^3$ per revolution. Consequently, the volumetric flow rate in the ER configuration is given by $Q_{MP} = V_{MP}n_{MP}$, where n_{MP} represents the rotational speed of the melt pump. In ER-IS, the throughput of the single-screw extruder with the smooth intake zone is strongly dependent on the back-pressure, and thus, the volumetric flow rate can no longer be evaluated directly. Hence, we developed a heuristic regression model to predict the mass output of the extruder based on two key input parameters: the screw rotation speed and the back-pressure at the screw tip. To generate the dataset required for modeling the screw characteristic line, a series of mass output experiments were conducted by systematically varying the screw speed and adjusting the

back-pressure using the bypass valve, as summarized in Table S1 in the supplementary material. At each design point, experiments were conducted using nine different screw speeds and four different back-pressures—covering a wide range of operating conditions of the extruder. For each combination of these parameters, four separate weight measurements were taken, each during a 36 s period of steady-state extrusion. The data collected were then processed using the HeuristicLab open-source software, in which symbolic regression was applied to derive a predictive output model [34]. Similar approaches have already been presented by Marschik *et al.* [35] and Hammer *et al.* [36].

The optimal symbolic regression model for predicting mass output was derived using the Offspring Genetic Algorithm (OSGA) within HeuristicLab 3.3.16. The key algorithmic parameters were as follows: Maximum Generations = 125, Mutation Probability = 20%, Population Size = 300, Selected Parents = 200, Elites = 1, and the operations allowed on constants and variables were addition, subtraction, multiplication, division, and exponential functions. The resulting symbolic model Eq. (10), developed for PE-HD at 200 °C, includes nine coefficients and fits the data well, achieving a coefficient of determination R^2 exceeding 0.99 for both the training and test datasets. The obtained model constants $c_0 - c_8$ and the design of experiment—which was used as a basis for the data based modeling—are listed in the supplementary material,

$$\dot{m}(n,p) = \left(\frac{c_0 \cdot n}{\left(\left(\left(\log\left((c_1 \cdot n)^2\right) - (c_2 \cdot p - c_3)\right) + c_4 \cdot n\right) + (c_5 \cdot p)^2\right) \cdot c_6} \cdot c_7 + c_8 \right). \tag{10}$$

The heuristic model, described by Eq. (10), is plotted alongside the measured values for comparison in Fig. 4(a). For further assessment of the model's predictive accuracy, Fig. 4(b) shows a scatterplot that compares the predicted and actual mass output values.

IV. RESULTS AND DISCUSSION

A. Injection of diluent and pressure fluctuations

Figure 5 plots the temperature-corrected pressure loss in the slit rheometer along the measurement length $L = 75$ mm as a function of time. At the onset of diluent injection (t_0), a slight initial increase in pressure loss is observed, which we attribute to the additional volumetric flow introduced by the HPLC pump. As soon as the first diluted polymer exits the slit die, a lower equilibrium pressure loss is established. This trend continues until a steady-state level is reached at t_1. Upon completion of diluent injection at t_2, the pressure loss increases immediately and then gradually returns to its initial value, which corresponds to that of the undiluted polymer melt. As the time stamps of these events cannot be predicted, all measurements must be corrected manually to remove erroneous values and obtain a more accurate mean value.

In addition to the overall pressure-loss behavior, minor fluctuations were observed throughout the measurement. To increase data reliability, only the equilibrium pressure values were considered for further evaluation. These were averaged using the arithmetic mean, and the standard deviation was calculated to assess data variability.

B. Validation of the absence of wall slip

Short-chain *n*-alkanes such as *n*-decane are also known to act as external plasticizers or lubricants. In this role, they do

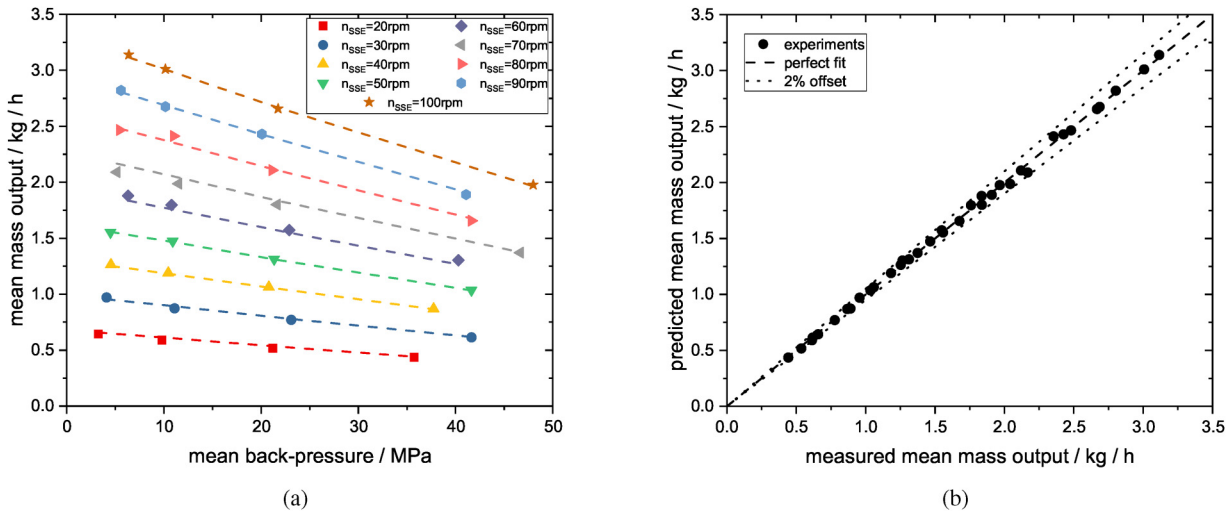

(a) (b)

FIG. 4. (a) Screw characteristic curve for PE-HD at 200 °C. Dashed lines and symbols show the results of the heuristic model and the experiments, respectively. (b) Measured versus predicted mass output (heuristic model at 200 °C). Points mark the experiments, the dashed line represents a perfect fit of $R^2 = 1$ and the dotted lines indicate a 2% offset from the perfect fit.

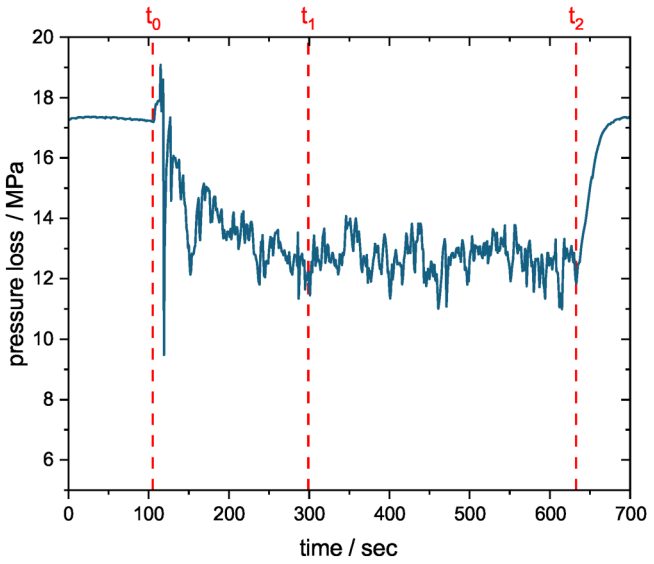

FIG. 5. Time-dependent pressure fluctuations during diluent injection. The experiment shown was done in ER at 200 °C with a PE-HD volume flow rate of 0.304 cm^3/s and a diluent (C10) volume flow rate of 2.091 ml/min resulting in a diluent concentration of 8.3% at an approximate wall shear rate of 55.3 s^{-1}.

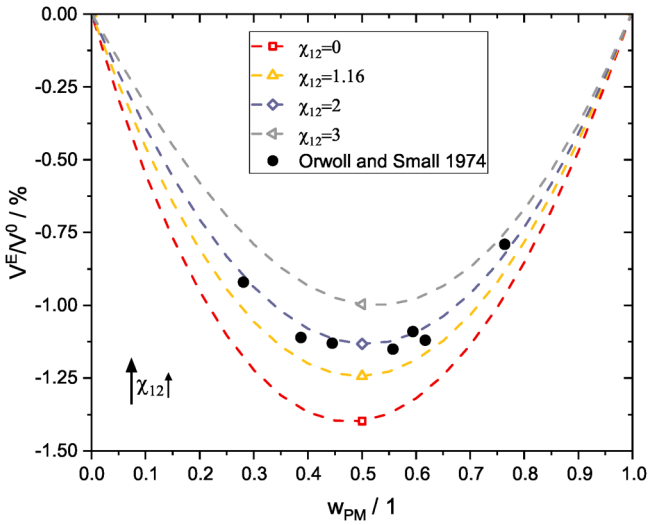

FIG. 6. Excess volume ratios V^E/V^0 for various values of the interaction parameter χ_{12} at 150 °C.

not primarily plasticize the polymer bulk but may reduce interfacial adhesion, thereby promoting wall slip during flow. Since wall slip would also lead to an apparent viscosity reduction and a decrease in pressure loss, it was necessary to verify that the observed effects did not originate from this mechanism.

Wall-slip detection was performed using a parallel-plate rheometry at varying gap heights, following the procedure proposed by Yoshimura and Prud'homme [32]. If a slip occurs, the measured torque decreases at smaller gaps due to the dependence of slip velocity on wall shear stress. However, for the investigated polymer–diluent systems, the torque response did not decrease with decreasing gap height, which indicates that no wall slip occurred under the applied conditions.

Although these results provide strong evidence against wall slip in the current experiments, complementary extrusion rheometry tests using dies of different slit heights are planned as a more direct validation.

C. Validation of pressure linearity

As described in Subsection III B, verifying the linearity of the pressure profile is essential to ensuring accurate rheological measurements. A least-squares approximation was applied to the pressure data recorded by the three transducers, fitting a linear curve to each measurement. This process yielded mean coefficients of determination R^2 of at least 0.99 for all cases. This confirms that the pressure along the slit die followed a linear trend, which indicates fully developed flow and the absence of secondary effects on viscosity reduction, such as viscous dissipation, pressure dependency, and bubble formation.

D. Assumption of volume additivity

Due to excess volume effects, the total volume of a binary liquid mixture is generally not strictly additive. However, for the present study, a linear mixing rule was assumed. This is supported by the findings of Orwoll and Small [37], who investigated the excess volume of mixing for PE and *n*-decane. Their study demonstrated that the ratio of excess volume V^E to the ideal mixed volume V^0—as predicted by a linear mixing rule—is in the order of 10^{-2}.

The maximum deviation from ideal volume additivity was reported at a polymer weight fraction of $w_{PM} = w_{10} = 0.5$, where the weight fractions of PE and *n*-decane are equal. Even at this concentration, which exceeds the highest diluent fraction investigated in the present study, the deviation does not exceed 1.2%. Furthermore, the excess volume effect

TABLE I. Design of experiments for ER at 240 °C.

Volume flow of melt pump Q_{MP} (cm^3/s)	Volume flow of diluent pump Q_{DP} (ml/min)	Resulting diluent mass concentration (%)	Approximate wall shear rate $\dot{\gamma}$ (1/s)	Viscosity at approx. wall shear rate η (Pa s)	Normalized viscosity $\tilde{\eta}$ (1)
0.42	0.00	0.0	68.7	1560.4	1.02
	0.67	2.0	70.4	1290.7	0.86
	1.37	4.0	72.2	1131.0	0.77
	2.88	8.0	76.2	845.8	0.60
	4.58	12.1	80.6	785.8	0.58
	6.49	16.4	85.6	654.0	0.50
	8.66	20.7	91.2	647.0	0.52

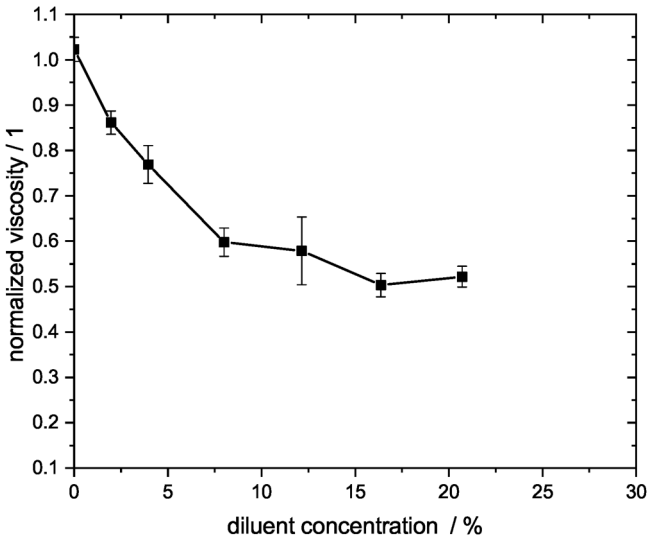

FIG. 7. Influence of diluent concentration on the normalized viscosity in ER.

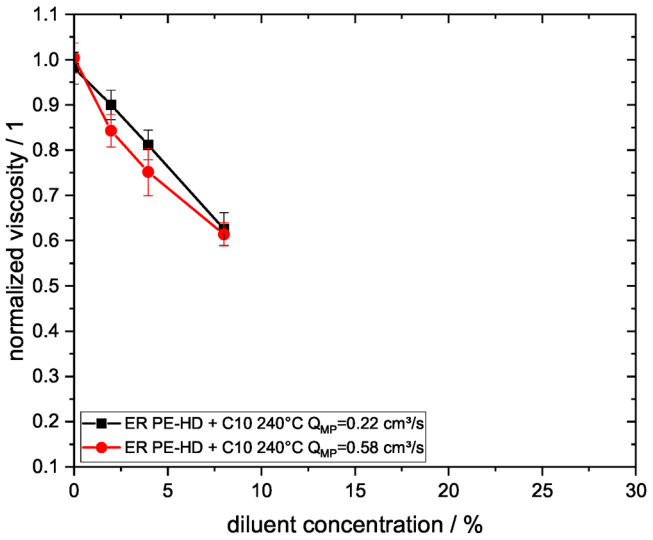

FIG. 8. Comparison of viscosity measurements at various volume flow rates of the melt pump in ER.

decreases with increasing pressure conditions that are relevant in polymer processing. Given the small size of these deviations and the fact that polymer processing conditions favor volume additivity, we considered the use of a linear mixing rule for volume estimation to be justified in this study. Figure 6 presents excess volume ratios V^E/V^0 for various interaction parameters χ_{12}, ranging from 0 to 3. For comparison, experimental data from Orwoll and Small [37] are included, with their reported interaction parameter of $\chi_{12} = 1.16$.

E. Slit rheometry with injection after melt pump

The experimental conditions for all measurements conducted using the melt pump are summarized in Table I. The total volumetric flow rate was determined based on the linear mixing rule, which was then used to determine the corresponding shear rate and viscosity.

Figure 7 shows the normalized viscosity of PE-HD as a function of *n*-decane concentration for extrusion rheometry (ER) experiments with downstream diluent injection. A pronounced viscosity reduction was observed up to approximately 20% diluent, beyond which the effect leveled off and only minor changes were detected. This apparent saturation behavior was not observed in parallel-plate measurements with offline saturation, where viscosity continued to decrease with increasing diluent content ($c > 50\%$). The discrepancy indicates that the saturation trend in ER is likely an limitation of the setup, most plausibly caused by incomplete mixing downstream of the injection point.

Further analysis revealed that the normalized viscosity also depended on the volumetric flow rate of the melt pump, as illustrated in Fig. 8. At higher flow rates, the measured viscosity was consistently lower, which suggests that the residence time and shear conditions in the static mixer were insufficient to ensure complete homogenization. This highlights that, besides concentration, the mixing efficiency strongly influences the effective viscosity reduction in ER experiments.

TABLE II. Design of experiments for investigating the influence of the revolutions of the SSE in ER-IS at 200 °C.

Predicted volume flow of the extruder Q_{pred} (cm³/s)	Volume flow of diluent pump Q_{DP} (ml/min)	Resulting diluent mass concentration (%)	Approximate wall shear rate $\dot{\gamma}$ (1/s)	Viscosity at approx. wall shear rate η (Pa s)	Normalized viscosity $\tilde{\eta}$ (1)
0.19	0.00	0.0	29.7	3716.3	0.92
0.20	0.60	3.9	33.4	2654.8	0.72
0.21	1.34	7.9	36.8	1993.3	0.58
0.22	2.22	12.1	40.4	1462.4	0.45
0.22	3.23	16.2	44.0	1104.3	0.36
0.23	4.39	20.5	47.7	864.4	0.30
0.23	5.72	24.8	51.8	669.1	0.25
0.24	7.28	29.3	56.4	524.9	0.21
0.66	0.00	0.0	104.8	1479.7	0.92
0.70	2.10	3.9	117.2	1130.5	0.76
0.75	4.73	7.8	131.7	813.8	0.60
0.79	7.95	11.9	146.5	600.4	0.48
0.81	10.00	14.2	154.9	510.1	0.42

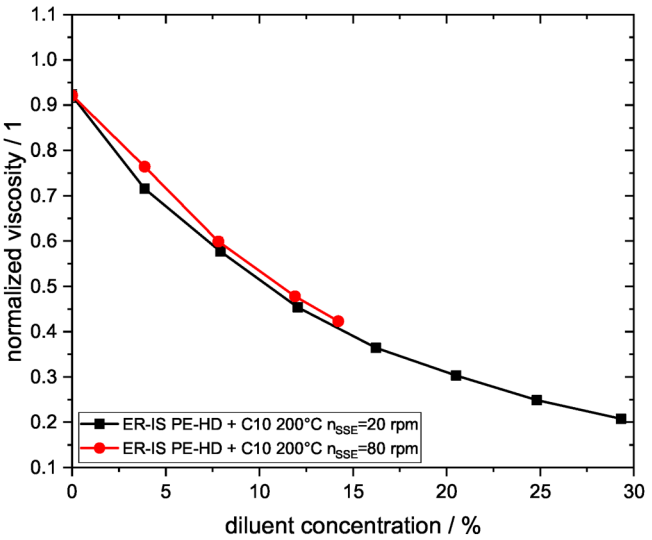

FIG. 9. Influence of revolutions of the single-screw extruder n_{SSE} in ER-IS. Error bars representing the standard deviations are smaller than the symbol size.

The findings emphasize the need for improved injection and mixing strategies to ensure homogeneous diluent distribution in extrusion rheometry. Additionally, experiments at higher diluent contents were restricted by the operational limits of the HPLC pump, which provides a maximum volumetric flow rate of 10 ml min^{-1} and a maximum operating pressure of 400 bar.

F. Slit rheometry without melt pump

In the absence of a melt pump, the volumetric flow rate is no longer under direct control and must instead be predicted based on extruder operating conditions. The mass output of the extruder, $\dot{m}_{pred}$, is determined primarily by two input parameters: the screw rotation speed n and the back-pressure at the screw tip p. Assuming an incompressible melt density ρ_m allows the volumetric flow rate Q_{pred} to be estimated as follows:

$$Q_{pred} = \frac{\dot{m}_{pred}}{\rho_m}. \tag{11}$$

Compared to the setup utilizing a melt pump, where volumetric flow rates are predefined, this configuration introduces additional complexities. Since the extruder mass output depends on the back-pressure at the screw tip, which is influenced by the viscosity of the polymer–diluent mixture, a feedback loop is created when targeting specific diluent concentrations. Maintaining control over the concentration levels requires either estimation of the back-pressure reduction or implementation of real-time adjustments to the diluent flow rate.

Due to limitations in the extruder instrumentation and the absence of real-time flow measurement, the first approach—estimating the back-pressure reduction—was selected. This was done based on experimental data obtained under comparable conditions. As a result, the targeted diluent concentrations were not perfectly achieved, but the approximation was considered sufficient for the objectives of this study.

The experimental design used to investigate the influence of shear rate on the rheological behavior in the ER-IS configuration is summarized in Table II, and the corresponding results are presented in Fig. 9. The data reveal that changes in shear rate had a less pronounced impact on the viscosity measured in the ER-IS setup than that in the ER configuration. This observation suggests that the enhanced in-line mixing achieved by direct injection into the extruder significantly mitigated shear-rate dependency, thereby contributing to more stable and reproducible rheological measurements.

The experimental plan for the comparison of ER and ER-IS is presented in Table III.

To facilitate this comparison, the normalized viscosity is plotted as a function of diluent concentration in Fig. 10. It is evident that when the diluent was introduced directly into the extruder (ER-IS), the saturation concentration threshold was higher than for injection downstream of the melt pump (ER). However, at lower concentrations, both approaches yielded comparable viscosity reductions.

Additionally, the standard deviation of the viscosity measurements was lower for ER-IS, which indicates that the extruder provided superior mixing performance compared to the static mixers used in ER. This improved homogeneity leads to more reliable rheological data and constitutes another advantage of in-extruder injection.

The validation of the measurement method is complete, and the viscosity-shear rate behavior at varying diluent concentrations can be systematically analyzed. Figures 11(a) and 11(b) illustrate pronounced viscosity reductions at 200 and 240 °C, respectively, with a 25% diluent concentration resulting in

TABLE III. Design of experiments for ER-IS for the comparison with ER at 240 °C.

Predicted volume flow of the extruder Q_{pred} (cm^3/s)	Volume flow of diluent pump Q_{DP} (ml/min)	Resulting diluent mass concentration (%)	Approximate wall shear rate $\dot{\gamma}$ (1/s)	Viscosity at approx. wall shear rate η (Pa s)	Normalized viscosity $\tilde{\eta}$ (1)
0.19	0.00	0.0	30.0	2795.6	1.00
0.12	0.60	3.7	33.0	2181.2	0.84
0.21	1.34	7.6	36.5	1646.3	0.68
0.22	2.22	11.5	40.2	1224.6	0.54
0.23	3.23	15.4	44.2	883.2	0.42
0.23	4.39	19.4	48.2	653.0	0.33

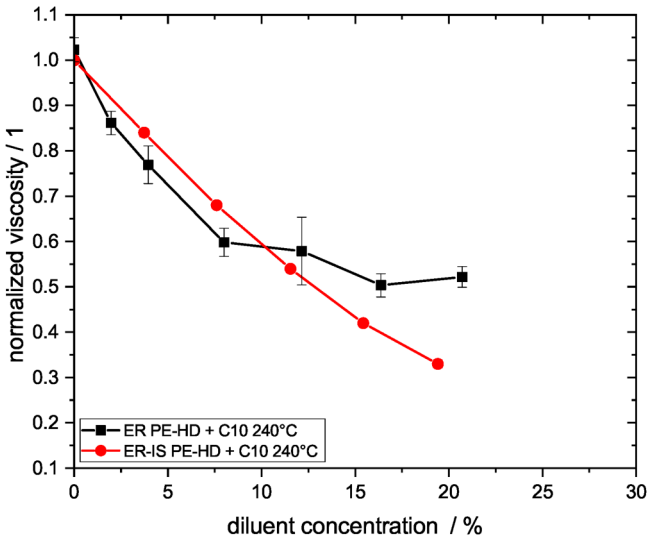

FIG. 10. Viscosity reduction for injection after melt pump (ER) and injection in extruder (ER-IS). Error bars representing the standard deviations are obscured by the symbols.

an approximate 70% decrease in viscosity. Our method enables measurement at intermediate shear rates ranging from 10 to 200 s^{-1}, bridging the gap between conventional low- and high-shear rheological techniques. Note that each data point in the figures represents an individual experiment, which means that the targeted diluent concentrations, as indicated in the legend, were not always precisely achieved. The actual concentration levels used for each measurement, together with the corresponding design of experiments, are summarized in the supplementary material. Detailed tables are provided for 200 (Table S2 in the supplementary material) and 240 °C (Table S3 in the supplementary material). Accounting for these deviations and enabling a more rigorous analysis of viscosity reduction require a viscosity–concentration model. This modeling approach, which aims to eliminate, among other things, the influence of concentration fluctuations.

V. CONCLUSION

A slit-rheometry-based setup was developed to systematically investigate the flow behavior of diluted polymer melts under controlled processing conditions. A key feature of the design is the flexibility in diluent injection, enabling direct assessment of how injection position and extrusion parameters influence viscosity reduction. A heuristic regression model for screw throughput provided robust control of the volumetric flow rate despite the inherent complexities of single-screw extrusion.

Using HD-PE with *n*-decane as a representative system, it was confirmed that dilution induces a significant drop in melt viscosity. Particular attention was given to the potential occurrence of wall slip, since short *n*-alkanes such as *n*-decane can act as external lubricants. This was evaluated by a parallel-plate rheometry of saturated polymer–diluent disks at varying gap heights. The torque response did not decrease with decreasing gap size, indicating the absence of wall slip under the applied conditions. Nevertheless, additional extrusion experiments with varying slit heights are planned to further substantiate this finding.

The magnitude of viscosity reduction strongly depended on the injection position. Direct injection into the extruder barrel improved mixing efficiency and, unlike the downstream ER configuration, did not exhibit saturation at higher diluent concentrations. This observation, consistent with parallel-plate and ER-IS measurements, underscores the decisive role of mixing in achieving homogeneous diluent distribution.

Two main limitations must be acknowledged. First, viscosity data are highly sensitive to precise temperature control, reflecting both the throughput behavior of the extruder and the strong temperature dependence of polymer melts. Second, the apparent saturation observed in the ER setup was attributed to incomplete in-line mixing rather than intrinsic material behavior; notably, this artifact was absent when using the ER-IS configuration.

Future work should address these limitations through real-time concentration monitoring. Emerging spectroscopic methods, such as terahertz spectroscopy [38], offer promising

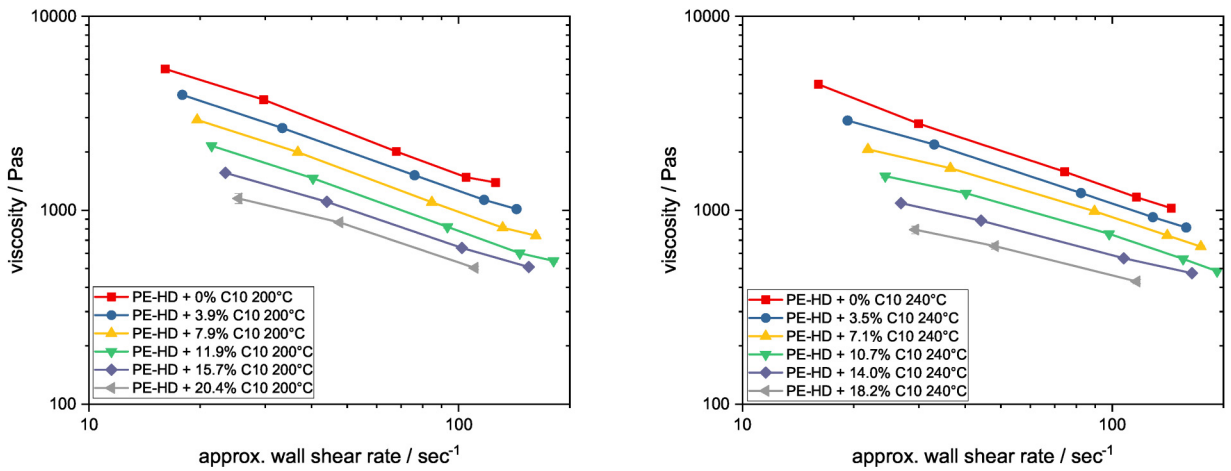

(a) (b)

FIG. 11. Influence of the diluent concentration on the viscosity at (a) 200 and (b) 240 °C.

opportunities for in-line quantification of diluent content, though their integration will require systematic validation.

Overall, the results consistently demonstrated a vertical viscosity shift with increasing diluent content, confirming dilution as a robust strategy for tailoring polymer melt rheology. The presented methodology establishes a reproducible framework for studying viscosity reduction and provides the foundation for predictive modeling of polymer–diluent systems. Such predictive capabilities are directly relevant to industrial processes ranging from extrusion and devolatilization to polymer foaming and plasticization, where controlled viscosity reduction is essential for process design and optimization.

SUPPLEMENTARY MATERIAL

See the supplementary material for the used antoine fit parameters, the heuristic throughput model parameters, and design of experiments.

ACKNOWLEDGMENTS

The authors acknowledge support through the FTI initiative circular economy "circPLAST-mr," funded by the BMK (Federal Ministry for Climate, Environment, Energy and Innovation) and the FFG (Austrian Research Promotion Agency)—Funding No. 889843.

During the preparation of this work, the authors used Chat GPT-5 in order to increase readability. After using this tool, the authors reviewed and edited the content as needed and employed a professional editor and take full responsibility for the content of the published article.

AUTHOR DECLARATIONS

Conflict of Interest

The authors have no conflicts to disclose.

DATA AVAILABILITY

The data that support the findings of this study are available from the corresponding author upon reasonable request.

REFERENCES

[1] Spencer, R. S., and J. L. Williams, "Concentrated solution viscosity of polystyrene," J. Colloid Sci. **2**, 117–129 (1947).

[2] Fujita, H., and E. Maekawa, "Viscosity behavior of the system polymethyl acrylate and diethyl phthalate over the complete range of composition," J. Phys. Chem. **66**, 1053–1058 (1962).

[3] Graessley, W. W., "Molecular entanglement theory of flow behavior in amorphous polymers," J. Chem. Phys. **43**, 2696–2703 (1965).

[4] Nishimura, N., "Viscosities of concentrated polymer solutions," J. Polym. Sci. Part A: Gen. Pap. **3**, 237–253 (1965).

[5] Brockmeier, N. F. and S. P. Westphal, "Viscometric behavior of high-density polyethylene solutions at high temperatures," Polym. Eng. Sci. **14**, 782–790 (1974).

[6] Ide, Y., and J. L. White, "Rheological phenomena in polymerization reactors: Rheological properties and flow patterns around agitators in polystyrene–styrene solutions," J. Appl. Polym. Sci. **18**, 2997–3018 (1974).

[7] Mendelson, R. A., "A method for viscosity measurements of concentrated polymer solutions in volatile solvents at elevated temperatures," J. Rheol. **23**, 545–556 (1979).

[8] Foster, R. W. and J. T. Lindt, "Concentration, temperature and deformation effects in concentrated polymer solutions with volatile solvents," Polym. Eng. Sci. **27**, 1292–1299 (1987).

[9] Fernández-Ronco, M. P., R. Hufenus, and M. Heuberger, "Effect of pressurized CO_2 and N_2 on the rheology of PLA," Eur. Polym. J. **112**, 601–609 (2019).

[10] Han, C. D., and C.-Y. Ma, "Rheological properties of mixtures of molten polymer and fluorocarbon blowing agent. II. Mixtures of polystyrene and fluorocarbon blowing agent," J. Appl. Polym. Sci. **28**, 851–860 (1983).

[11] Royer, J. R., J. M. DeSimone, and S. A. Khan, "High-pressure rheology and viscoelastic scaling predictions of polymer melts containing liquid and supercritical carbon dioxide," J. Polym. Sci. Part B: Polym. Phys. **39**, 3055–3066 (2001).

[12] Kwag, C., Rheology of molten polystyrene with dissolved gases, Ph.D. thesis, Wayne State, 1998.

[13] Gerhardt, L. J., C. W. Manke, and E. Gulari, "Rheology of polydimethylsiloxane swollen with supercritical carbon dioxide," J. Polym. Sci. Part B: Polym. Phys. **35**, 523–534 (1997).

[14] Gerhardt, L. J., A. Garg, C. W. Manke, and E. Gulari, "Concentration-dependent viscoelastic scaling models for polydimethysiloxane melts with dissolved carbon dioxide," J. Polym. Sci. Part B: Polym. Phys. **36**, 1911–1918 (1998).

[15] Lee, M., C. Tzoganakis, and C. B. Park, "Extrusion of PE/PS blends with supercritical carbon dioxide," Polym. Eng. Sci. **38**, 1112 (1998).

[16] Ma, C.-Y., and C. Dae Han, "Measurement of the viscosities of mixtures of thermoplastic resin and fluorocarbon blowing agent," J. Cell. Plast. **18**, 361–370 (1982).

[17] Areerat, S., T. Nagata, and M. Ohshima, "Measurement and prediction of LDPE/CO_2 solution viscosity," Polym. Eng. Sci. **42**, 2234–2245 (2002).

[18] Handge, U. A., and V. Altstädt, "Viscoelastic properties of solutions of polystyrene melts and carbon dioxide: Analysis of a transient shear rheology approach," J. Rheol. **56**, 743–766 (2012).

[19] Qin, X., M. R. Thompson, A. N. Hrymak, and A. Torres, "Rheology studies of polyethylene/chemical blowing agent solutions within an injection molding machine," Polym. Eng. Sci. **45**, 1108–1118 (2005).

[20] Akkarachittoor, N. S., A. L. Fricke, and J. D. Small, "Dual chamber capillary viscometer for viscosity measurements of concentrated polymer solutions at elevated temperatures," Rev. Sci. Instrum. **57**, 1182–1184 (1986).

[21] Westover, R. F., "Effect of hydrostatic pressure on polyethylene melt rheology," Polym. Eng. Sci. **1**, 14–20 (1961).

[22] Mackley, M. R., R. T. J. Marshall, and J. B. A. F. Smeulders, "The multipass rheometer," J. Rheol. **39**, 1293–1309 (1995).

[23] Mackley, M. R., and P. H. J. Spitteler, "Experimental observations on the pressure-dependent polymer melt rheology of linear low density polyethylene, using a multi-pass rheometer," Rheol. Acta **35**, 202–209 (1996).

[24] Richards, W. D., and R. K. Prud'Homme, "A rheometer for concentrated polymer solutions containing volatile solvents," Polym. Eng. Sci. **27**, 294–302 (1987).

[25] Royer, J. R., Y. J. Gay, M. Adam, J. M. DeSimone, and S. A. Khan, "Polymer melt rheology with high-pressure CO_2 using a novel magnetically levitated sphere rheometer," Polymer **43**, 2375–2383 (2002).

[26] Royer, J. R., Y. J. Gay, J. M. Desimone, and S. A. Khan, "High-pressure rheology of polystyrene melts plasticized with CO_2: Experimental measurement and predictive scaling relationships," J. Polym. Sci. Part B: Polym. Phys. **38**, 3168–3180 (2000).

[27] Lee, M., C. B. Park, and C. Tzoganakis, "Measurements and modeling of PS/supercritical CO_2 solution viscosities," Polym. Eng. Sci. **39**, 99–109 (1999).

[28] Antoine, C., "Tensions des vapeurs; nouvelle relation entre les tensions et les températures: [Vapor pressure: A new relationship between pressure and temperature]," C. R. Seances Acad. Sci. **107**(681), 836 (1888).

[29] Kastner, E., "Zeit-Konzentration-Superposition am Beispiel konzentrierter Polyethylenlösungen," Ph.D. thesis, Johannes Kepler Universität Linz, 1996.

[30] Linstrom, P. J., and W. G. Mallard, "NIST chemistry webbook," NIST standard reference database number 69.

[31] Han, C. D., *Rheology and Processing of Polymeric Materials* (Oxford University Press, Oxford, 2007).

[32] Yoshimura, A., and R. K. Prud'homme, "Wall slip corrections for couette and parallel disk viscometers," J. Rheol. **32**, 53–67 (1988).

[33] Schümmer, P., and R. H. Worthoff, "An elementary method for the evaluation of a flow curve," Chem. Eng. Sci. **33**, 759–763 (1978).

[34] Wagner, S., G. Kronberger, A. Beham, M. Kommenda, A. Scheibenpflug, E. Pitzer, S. Vonolfen, M. Kofler, S. Winkler, V. Dorfer, and M. Affenzeller, "Architecture and design of the heuristiclab optimization environment," in *Advanced Methods and Applications in Computational Intelligence*, Topics in Intelligent Engineering and Informatics Vol. 6, edited by R. Klempous, J. Nikodem, W. Jacak, and Z. Chaczko (Springer International, Heidelberg, 2014), pp. 197–261.

[35] Marschik, C., M. Dörner, W. Roland, J. Miethlinger, V. Schöppner, and G. Steinbichler, "Application of network analysis to flow systems with alternating wave channels: Part A (pressure flows)," Polymers **11**, 1488 (2019).

[36] Hammer, A., W. Roland, M. Zacher, S. Kohl, and G. Berger–Weber, "Experimental validation of non–Newtonian stratified co-extrusion prediction models using a digital process twin," Polym. Eng. Sci. **62**, 3902–3922 (2022).

[37] Orwoll, R. A., and J. A. Small, "Volume changes of mixing and excess coefficients of thermal expansion for solutions of polymethylene in n-decane," Macromolecules **6**, 755–757 (1973).

[38] Fosodeder, P., M. Pfleger, K. Rahman, T. Dutton, S. Cozien-Cazuc, S. van Frank, and C. Rankl, "Fast terahertz reflection imaging for in-line detection of delaminations in glass fiber-reinforced polymers," Sensors **25**, 851 (2025).